12-14-2021

Revised semiempirical approach to predict the occurrence of twinning in titanium alloys

Chirag Dhirajlal Rabadia
Edith Cowan University

Syed Faraz Jawed

Jincheng Wang
Edith Cowan University

Milind Siddhpura

Arti Siddhpura

10.1021/acsomega.1c05474
Rabadia, C. D., Jawed, S. F., Wang, J., Siddhpura, M., & Siddhpura, A. (2021). Revised semiempirical approach to predict the occurrence of twinning in titanium alloys. ACS Omega, 6(49), 34056-34064.
https://doi.org/10.1021/acsomega.1c05474

ACS OMEGA

http://pubs.acs.org/journal/acsodf

Article

Revised Semiempirical Approach to Predict the Occurrence of Twinning in Titanium Alloys

Chirag Dhirajlal Rabadia,* Syed Faraz Jawed, Jincheng Wang, Milind Siddhpura, and Arti Siddhpura

Cite This: *ACS Omega* 2021, 6, 34056–34064

Read Online

ACCESS | Metrics & More | Article Recommendations

ABSTRACT: A revised semiempirical approach, considering the average values of the valence electron to atom ratio $(e/\overline{a})$ and a difference in atomic radii of alloying element/s and the base element $(\Delta\overline{r})$, is proposed to predict the twin formation in titanium alloys. The revised $e/\overline{a}$ versus $\Delta\overline{r}$ diagram is plotted, considering the reported results of 90 titanium alloys fabricated using various processing methods. A new twin/slip boundary has been plotted and recommended based on the revised $e/\overline{a}$ versus $\Delta\overline{r}$ diagram. The conventional maximum limit reported for the twinning in titanium alloys is $e/\overline{a}$ = 4.20; however, it has been found that twinning in titanium alloys is possible up to the $e/\overline{a}$ of 4.30.

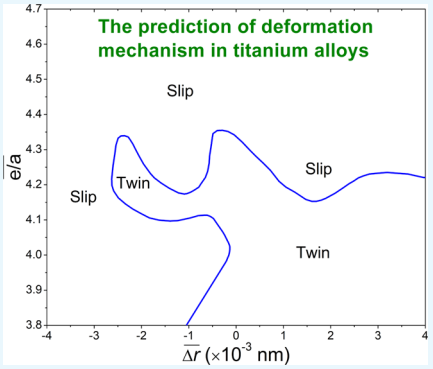

1. INTRODUCTION

The last decade has witnessed exponential growth in the development of titanium alloys produced using various thermomechanical processing routes, powder metallurgy, selective laser melting, spark plasma sintering, and many other fabrication techniques for their use in biomedical, aerospace, power plant, and automobile industries.[1,2] A wide range of mechanical, corrosion, and biological properties can be obtained by appropriately tailoring the microstructure of titanium alloys.[3,4] Each alloying element of titanium alloys reacts differently in varying microstructures and mechanical properties.[3,5,6] Therefore, each titanium alloy deforms differently from one another depending on the phases present in the microstructure and their structural parameters.[7,8] Furthermore, the type of deformation mechanism, for example, twin, slip and so forth, plays a vital role in tailoring the mechanical properties of titanium alloys.[9] Twin boundaries present in crystalline alloys improve dislocation storage ability.[10,11] Therefore, alloys that deform by a twin-dominating mechanism demonstrate low yield strength and large elongation/plasticity, whereas alloys that deform by a slip-dominating mechanism demonstrate high yield strength and less elongation/plasticity.[9] In general, twinning helps in achieving significant work hardening in alloys especially used for biomedical and many shape memory applications.[10,12]

Established literature acknowledges that twinning is fundamentally possible in lower-symmetry metals/metal alloys comprising body-centered cubic, hexagonal close-packed, and face-centered cubic structures.[12] Twinning in alloys may occur during deformation, phase transformation, and/or recrystallization by a homogeneous simple shearing of the parent/matrix lattice in alloys with low stacking fault energies.[12] Consequently, deformation twins possess many stacking faults with imperfect structures. Moreover, the chemical composition is one of the influencing factors in the occurrence of twinning in alloys because all the elements react differently in terms of either increasing or decreasing the grain size, the amount of interstitial or substitutional solutes, stacking fault energy, and so forth, and all these parameters also influence the occurrence of twinning.[10,12]

Twinning is a fundamental deformation mode in bcc metastable β titanium alloys.[13] Twinning improves work hardening properties in titanium alloys.[13] The mechanism which provides significant work hardening is known as twin-induced plasticity effect in titanium alloys.[13] Moreover, it has been reported that twining also increases strain in titanium alloys and creates obstacles in gliding dislocations.[13] The deformation mechanisms such as deformation mechanisms including {112}<111> twinning, {332}<113> twinning, and stress-induced α'' martensitic transformation usually remain evident in less stable β titanium alloys which display high work hardening, whereas the slip deformation mechanism remains evident in stable β titanium alloys which display poor ductility.[13] When considering the properties of eutectic alloys, it has been reported that slip

Received: October 1, 2021
Accepted: November 17, 2021
Published: December 2, 2021

systems also dominate in titanium-based (i.e., Ti−Si−Sn, Ti−Fe−Co, Ti−Fe, $Ti_{67.79}Fe_{28.36}Sn_{3.85}$, etc.),[14,15] aluminum-based (i.e., Al−3.1Ni, Al−17Cu, Al−12.2Si, etc.), copper-based (i.e., Cu−23.1MG, Cu−2.8Zr, Cu−Ge, Cu−26Ag, Cu−19.7B, Cu−CuZrGe, etc.), and nickel-based (i.e., Ni-32.5 atom %, Ni−W, Ni−Mo, Ni−Ni_3Si, etc.) eutectic alloys.[15]

Thermomechanical processing and manufacturing methods also influence the deformation properties of alloys.[8,16] Cryomilling is a new technology to produce high-strength nanomaterials, in which metallic powders are milled at cryogenic temperature to tailor the microstructure and mechanical behavior of materials.[17,18] The advantages of cryomilling include environmentally friendly nature, less contamination, rapid grain refinement, cost effectiveness, and large-scale production capability of various nanomaterials.[17] Other than additive manufacturing methods, cryomilling could also be crucial for producing titanium alloys to tailor various deformation and strengthening mechanisms.

The atomic radius and electronic parameters including the compositional average values of bond order ($B\bar{o}$), the d-orbital energy level ($M\bar{d}$) and the valence electron to atom ratio ($e/\bar{a}$) are important parameters in predicting the occurrence of twinning in alloys because these electronic parameters and atomic radii also affect the grain size, the amount of interstitial or substitutional solutes, and the stacking fault energy of alloys.[12,19] Abdel-Hady et al.[20] have proposed the extended phase stability diagram, based on the DV-Xα cluster method suggested by Morinaga et al.[21,22] considering the $B\bar{o}$ and $M\bar{d}$ parameters, which predicts the prospective phases, elastic modulus, and deformation mechanism for titanium alloys. Figure 1 shows the positions of Ti−35Nb−5Ta−7Zr,[23] Ti−35Zr−5Fe−2Mn,[24] Ti−33Zr−3Fe−2Cr,[25] Ti−33Zr−5Fe−2Cr,[25] Ti−33Zr−3Fe−4Cr,[25] Ti−1Fe,[26] and Ti−3Fe[26] on the extended phase stability diagram. It is worth noting that the alloys shown in Figure 1 do not lie in the slip region; however, these alloys demonstrate a slip-dominating deformation mechanism based on the experimental evidence reported in previous studies. This indicates that the DV-Xα cluster method is not completely effective in predicting the proposed deformation mechanism. Hence, there is still a need to develop an improved method for predicting the proposed deformation mechanism in titanium alloys.

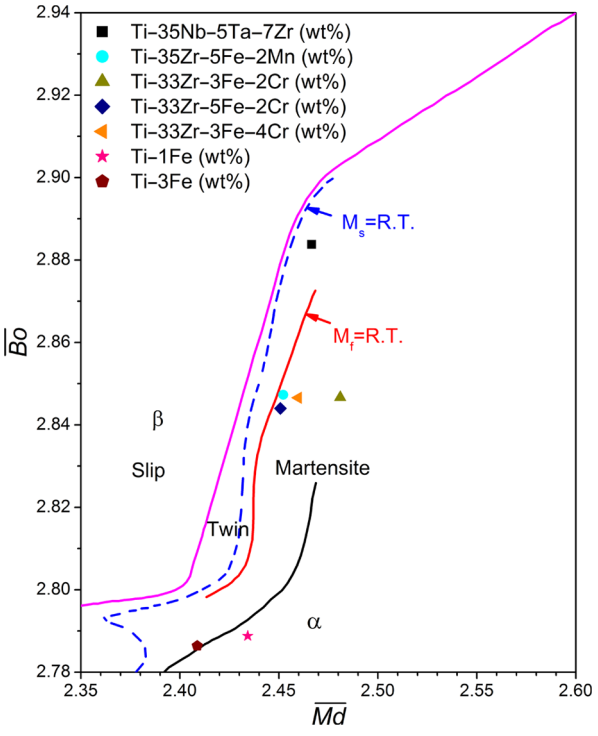

Figure 1. Positions of Ti−35Nb−5Ta−7Zr,[23] Ti−35Zr−5Fe−2Mn,[24] Ti−33Zr−3Fe−2Cr,[25] Ti−33Zr−5Fe−2Cr,[25] Ti−33Zr−3Fe−4Cr,[25] Ti−1Fe,[26] and Ti−3Fe[26] on the extended phase stability diagram.[20,27] [Reprinted in part with permission from Ref 20. Copyright 2006 ELSEVIER].

2. DETERMINATION OF PARAMETERS

The values of $B\bar{o}$ and $M\bar{d}$ were calculated using eqs 1 and 2, respectively.[27,28]

$$\overline{BO} = \sum x_i \cdot (Bo)_i \tag{1}$$

$$\overline{Md} = \sum x_i \cdot (Md)_i \tag{2}$$

Where x_i is atomic fraction (atomic weight/atomic mass) of the ith component in the alloy composition and $(Bo)_i$ and $(Md)_i$ are the respective values for the ith component.[21]

The values of $\Delta\bar{r}$ were determined using eq 3 in which titanium is considered as a base element.[5]

$$\overline{\Delta r} = \sum_{i}^{n} x_i (r_i - r_{Ti}) \tag{3}$$

where x_i is the atomic fraction, r_i is the metallic atomic radius of the ith element, r_{Ti} is the atomic radius of titanium, and n is the number of alloying elements. The values of $e/\bar{a}$ used were estimated using eq 4.[5]

$$\overline{e/a} = \sum_{i}^{n} x_i \cdot e_i \tag{4}$$

where x_i is the atomic fraction, e_i is the number of valence electrons of the ith element, and n is the number of alloying elements.

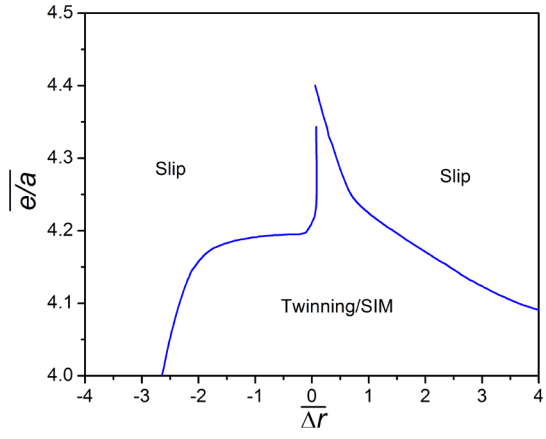

Figure 2. Semiempirical approach suggested by Wang et al.[19] considering the $e/\bar{a}$ (average valence electron to atom ratio) and $\Delta\bar{r}$ (atomic radii difference) values to understand the deformation mechanisms for solution-treated β titanium alloys. [Reprinted in part with permission from Wang et al.[19] Copyright 2018 ELSEVIER].

https://doi.org/10.1021/acsomega.1c05474
ACS Omega 2021, 6, 34056−34064

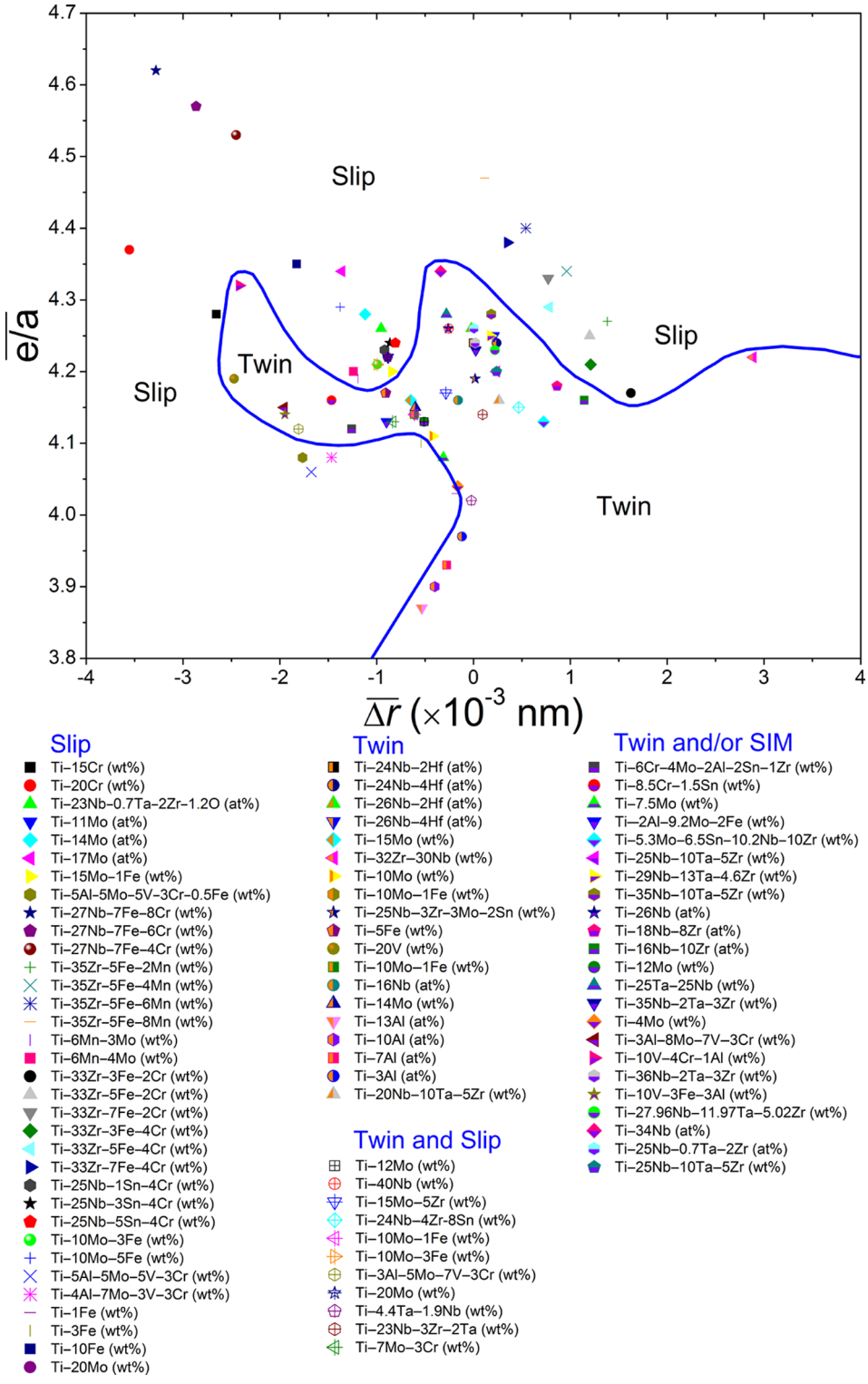

Figure 3. Revised $e/\overline{a}$ versus $\Delta\overline{r}$ diagram considering the results of titanium alloys reported in previous findings.[13,24−26,32−77]

3. RESULTS AND DISCUSSION

Wang et al.[19] have suggested a semiempirical approach considering the $e/\overline{a}$ and the compositional average of a difference in atomic radii of the base element and alloying element/s ($\Delta\overline{r}$) to understand the deformation mechanisms of β titanium alloys. Figure 2 shows the $e/\overline{a}$ versus $\Delta\overline{r}$ diagram proposed by Wang et al.,[19] which is valid only for solution-treated β titanium alloys and may not be valid for other titanium alloys produced using different processing methods. Investigations on the twin mechanism and the effects of twinning on the mechanical properties have been reported, based on the electron microscopic evidence, in an ample amount to date, which can be used to predict the occurrence of twinning by developing an improved semiempirical approach. Considering these points, the present work tries to propose a revised $e/\overline{a}$ versus $\Delta\overline{r}$ diagram for predicting the occurrence of twinning in titanium alloys considering the various fabrication/processing

https://doi.org/10.1021/acsomega.1c05474
ACS Omega 2021, 6, 34056−34064

Table 1. Values of $e/\bar{a}$ and $\Delta\bar{r}$ for Titanium Alloys (Processed Using Varied Processing/Fabrication Techniques) Showing the Slip Mechanism[a]

alloys	processing method	deformation mechanism	$e/\bar{a}$	$\Delta\bar{r} \times 10^{-3}$ nm	refs.
Ti−15Cr (wt %)	HR and CR	slip	4.28	−2.6554	32
Ti−20Cr (wt %)	HR and CR	slip	4.37	−3.5549	32
Ti−23Nb−0.7Ta−2Zr−1.2O (atom %)	ST	slip	4.26	−0.9546	33
Ti−11Mo (atom %)	annealed	slip	4.22	−0.8822	34
Ti−14Mo (atom %)	annealed	slip	4.28	−1.1199	34
Ti−17Mo (atom %)	annealed	slip	4.34	−1.3597	34
Ti−15Mo−1Fe (wt %)	HR and ST	slip	4.20	−0.8433	35
Ti−5Al−5Mo−5V−3Cr−0.5Fe (wt %)	ST	slip	4.08	−1.7660	36
Ti−27Nb−7Fe−8Cr (wt %)	cast	slip	4.62	−3.2816	37
Ti−27Nb−7Fe−6Cr (wt %)	cast	slip	4.57	−2.8661	37
Ti−27Nb−7Fe−4Cr (wt %)	cast	slip	4.53	−2.452	37
Ti−35Zr−5Fe−2Mn (wt %)	cast	slip	4.27	1.3826	24
Ti−35Zr−5Fe−4Mn (wt %)	cast	slip	4.34	0.9626	24
Ti−35Zr−5Fe−6Mn (wt %)	cast	slip	4.40	0.5400	24
Ti−35Zr−5Fe−8Mn (wt %)	cast	slip	4.47	0.1147	24
Ti−6Mn−3Mo (wt %)	HR and ST	slip	4.19	−1.1925	38
Ti−6Mn−4Mo (wt %)	HR and ST	slip	4.20	−1.2397	38
Ti−33Zr−3Fe−2Cr (wt %)	cast	slip	4.17	1.6260	25
Ti−33Zr−5Fe−2Cr (wt %)	cast	slip	4.25	1.2002	25
Ti−33Zr−7Fe−2Cr (wt %)	cast	slip	4.33	0.7714	25
Ti−33Zr−3Fe−4Cr (wt %)	cast	slip	4.21	1.2105	25
Ti−33Zr−5Fe−4Cr (wt %)	cast	slip	4.29	0.7824	25
Ti−33Zr−7Fe−4Cr (wt %)	cast	slip	4.38	0.3514	25
Ti−2SNb−1Sn−4Cr (wt %)	cast	slip	4.23	−0.9193	39
Ti−2SNb−3Sn−4Cr (wt %)	cast	slip	4.24	−0.8644	39
Ti−2SNb−5Sn−4Cr (wt %)	cast	slip	4.24	−0.8079	39
Ti−10Mo−3Fe (wt %)	HR and ST	slip	4.21	−0.9931	40
Ti−10Mo−5Fe (wt %)	HR and ST	slip	4.29	−1.3780	40
Ti−5Al−5Mo−5V−3Cr (wt %)	HR and ST	slip	4.06	−1.6761	41
Ti−4Al−7Mo−3V−3Cr (wt %)	HR and ST	slip	4.08	−1.4667	41
Ti−1Fe (wt %)	HR and annealed	slip	4.03	−0.1803	26
Ti−3Fe (wt %)	HR and annealed	slip	4.10	−0.5426	26
Ti−10Fe (wt %)	HR and annealed	slip	4.35	−1.826	42
Ti−20Mo (wt %)	HR	slip	4.22	−0.8872	43

[a]Note that hot-rolling, cold-rolling and solution treating are abbreviated as HR, CR, and ST, respectively.

methods such as casting, solution treating, annealing, ageing, hot rolling, cold rolling, powder metallurgy, and selective laser sintering.

Twin boundaries form as a result of simple shearing that occurs in the parent/base lattice as discussed above. The information on the shearing tendency of the lattice can be obtained based on the modulus of rigidity, which can be determined using the shear stress and shear strain of the parent lattice.[29] It has been reported that the modulus of rigidity increases as the $e/\bar{a}$ of alloys increases.[29] A relatively high shear stress is required to break the bonds between two atoms and, thereby, for shearing of the lattice when $e/\bar{a}$ increases and therefore, alloys possessing high $e/\bar{a}$ values show a slip-dominating mechanism.[19] However, the atomic size misfit effect also plays a crucial role in the occurrence of slip and twin boundaries. The atomic size misfit occurs when alloying element/s have either a higher or lower atomic radius than the base element according to the Hume-Rothery rules.[30] According to the established literature, the values of $e/\bar{a}$ are used to predict the β phase stability and the formation of intermetallic phases in titanium alloys,[1,25] whereas the values of $\Delta\bar{r}$ are used to predict the solid-solution strengthening effects and the deformation mechanisms based on the atomic size misfit phenomenon.[31]

Figure 3 depicts the revised $e/\bar{a}$ versus $\Delta\bar{r}$ diagram which has been proposed in the present work.

The regions of slip and twin in the revised $e/\bar{a}$ versus $\Delta\bar{r}$ diagram are found to be different than the regions of slip and twin presented in Figure 2. In the revised $e/\bar{a}$ versus $\Delta\bar{r}$ diagram, the results of around 90 titanium alloys have been considered for obtaining precise information on the regions of deformation mechanisms. Note that (i) the corresponding findings of these selected titanium alloys demonstrate the evidence of the deformation mechanism (i.e., slip/twin) based on the results of electron microscopy and (ii) the selected titanium alloys not only show a single β phase, but also show the other martensitic ($\alpha, \alpha', \alpha''$ ω) and intermetallic phases. Therefore, the revised $e/\bar{a}$ versus $\Delta\bar{r}$ diagram can be used for all the types of titanium alloys, that is, α, $\alpha + \beta$, and β alloys.

In the revised $e/\bar{a}$ versus $\Delta\bar{r}$ diagram, the titanium alloys demonstrating (i) twin, (ii) twin and slip, and (iii) twin and/or stress-induced martensite (SIM) are shown in a common twin region to obtain information on the occurrence of twinning in titanium alloys. In Figure 3, the titanium alloys demonstrating (i) only twin, (ii) twin and slip, and (iii) twin and/or SIM are shown using "half left filled with orange color", "open symbols with + sign", and "half down filled with purple color" symbols,

https://doi.org/10.1021/acsomega.1c05474
ACS Omega 2021, 6, 34056−34064

Table 2. Values of $e/\bar{a}$ and $\Delta\bar{r}$ for Titanium Alloys (Processed Using Varied Processing/Fabrication Techniques) Showing the Twin Mechanism[a]

alloys	processing method	deformation mechanism	$e/\bar{a}$	$\Delta\bar{r} \times 10^{-3}$ nm	refs.
Ti−24Nb−2Hf (atom %)	ST	twin	4.24	−0.0011	44
Ti−24Nb−4Hf (atom %)	ST	twin	4.24	0.2394	44
Ti−26Nb−2Hf (atom %)	ST	twin	4.26	−0.0221	44
Ti−26Nb−4Hf (atom %)	ST	twin	4.25	0.2115	44
Ti−15Mo (wt %)	HR and ST	twin	4.16	−0.6473	45
Ti−32Zr−30Nb (wt %)	CR and ST	twin	4.22	2.8876	46
Ti−10Mo (wt %)	HR and ST	twin	4.11	−0.4202	40
Ti−10Mo−1Fe (wt %)	HR and ST	twin	4.14	−0.6106	40
Ti−25Nb−3Zr−3Mo−2Sn (wt %)	HR and ST	twin	4.19	0.0169	47
Ti−5Fe (wt %)	HR and annealed	twin	4.17	−0.9064	42
Ti−20V (wt %)	HR and ST	twin	4.19	−2.4731	48
Ti−10Mo−1Fe (wt %)	HR and ST	twin	4.14	−0.6106	49
Ti−16Nb (at %)	HR and ST	twin	4.16	−0.1601	50
Ti−14Mo (wt %)	HR	twin	4.15	−0.6009	43
Ti−13Al (at %)	ST and annealed	twin	3.87	−0.5346	51
Ti−10Al (at %)	ST and annealed	twin	3.90	−0.4004	51
Ti−7Al (at %)	ST and annealed	twin	3.93	−0.2753	51
Ti−3Al (at %)	ST and annealed	twin	3.97	−0.1191	51
Ti−20Nb−10Ta−5Zr (wt %)	powder metallurgy and HT	twin	4.16	0.2626	52

[a]Note that hot-rolling, cold-rolling, solution treating, and heat treatment are abbreviated as HR, CR, ST, and HT, respectively.

Table 3. Values of $e/\bar{a}$ and $\Delta\bar{r}$ for Titanium Alloys (Processed Using Varied Processing/Fabrication Techniques) Showing the Twin and Slip Mechanisms[a]

alloys	processing method	deformation mechanism	$e/\bar{a}$	$\Delta\bar{r} \times 10^{-3}$ nm	refs.
Ti−12Mo (wt %)	ST	twin and slip	4.13	−0.5096	53
Ti−40Nb (wt %)	cold rolled and aged	twin and slip	4.26	−0.2557	54
Ti−15Mo−5Zr (wt %)	CR and ST	twin and slip	4.17	−0.2859	55
Ti−24Nb−4Zr−8Sn (wt %)		twin and slip	4.15	0.4670	76
Ti−10Mo−1Fe (wt %)	HR	twin and slip	4.14	−0.6106	56
Ti−10Mo−3Fe (wt %)	HR	twin and slip	4.21	−0.9931	56
Ti−3Al−5Mo−7V−3Cr (wt %)	HR and ST	twin and slip	4.12	−1.8076	41
Ti−20Mo (wt %)	ST	twin and slip	4.22	−0.8872	57
Ti−4.4Ta−1.9Nb (wt %)	ST	twin and slip	4.02	−0.0224	58
Ti−23Nb−3Zr−2Ta (wt %)	cast	twin and slip	4.14	0.0941	59
Ti−7Mo−3Cr (wt %)	CR and ST	twin and slip	4.13	−0.8354	77

[a]Note that hot-rolling, cold-rolling, and solution treating are abbreviated as HR, CR, and ST, respectively.

respectively. Moreover, the titanium alloys demonstrating only the slip mechanism are separated by a solid-blue line in Figure 3, and their positions are shown using solid symbols. The titanium alloys displaying the twin mechanism should have less β phase stability, whereas the titanium alloys displaying the slip mechanism should have stable β phase stability.[13]

The values of $e/\bar{a}$ and $\Delta\bar{r}$ for all the selected alloys are summarized in Tables 1−4 with necessary references. It has been reported in many findings that the slip usually forms in titanium alloys with $e/\bar{a}$ values greater than 4.20.[19] However, for titanium alloys shown in the slip region of Figure 3, the values of $e/\bar{a}$ vary from 4.03 to 4.62, whereas the values of $\Delta\bar{r}$ vary from -3.5×10^{-3} to 1.6×10^{-3} nm (Tables 2−4). This reveals that the slip is possible in titanium alloys with $e/\bar{a}$ values less than 4.20, which has been reported in alloys such as Ti−5Al−5Mo−5V−3Cr−0.5Fe (wt %),[36] Ti−6Mn−3Mo (wt %),[38] Ti−33Zr−3Fe−2Cr (wt %),[25] Ti−5Al−5Mo−5V−3Cr (wt %),[41] Ti−4Al−7Mo−3V−3Cr (wt %),[41] Ti−1Fe (wt %),[26] and Ti−3Fe (wt %).[26] The slip in these alloys possibly occurs due to atomic size misfit which increases the bonding strength between atoms. As a result, atomic movements become difficult which allows slip deformation instead of twin in these alloys. This phenomenon also suggests the importance of atomic size misfit in terms of $\Delta\bar{r}$ in the deformation of titanium alloys.

Furthermore, for titanium alloys shown in the twin region of Figure 3, the values of $e/\bar{a}$ vary from 3.87 to 4.34 and the values of $\Delta\bar{r}$ vary from -2.7×10^{-3} to 2.8×10^{-3} nm (Table 1). Out of all the titanium alloys demonstrating twinning in Figure 3, 81.5% of titanium alloys possess the $e/\bar{a}$ and $\Delta\bar{r}$ values that range from 4.10 to 4.30 and -1×10^{-3} to 1×10^{-3} nm, respectively. This indicates that the chances of twinning in titanium alloys remain high for the $e/\bar{a}$ values from 4.10 to 4.30 and the $\Delta\bar{r}$ values from -1×10^{-3} to 1×10^{-3} nm. Many findings have concluded that the possibility of twinning in titanium alloys remains high for $e/\bar{a}$ values not exceeding 4.20.[19] Consequently, the $e/\bar{a}$ value of 4.20 is believed to be the maximum limit for the occurrence of twinning because Coulombic forces between two positive ions increase as $e/\bar{a}$ increases, and thereby, the shearing of the lattice becomes difficult. However, the shearing of the lattice also depends on the atomic size misfit other than $e/\bar{a}$. Hence, if titanium alloys possess $e/\bar{a}$ values greater than 4.20, but possess the $\Delta\bar{r}$ close to 0 nm in the twin region shown in Figure 3, then

https://doi.org/10.1021/acsomega.1c05474
ACS Omega 2021, 6, 34056−34064

Table 4. Values of $e/\bar{a}$ and $\Delta\bar{r}$ for Titanium Alloys (Processed Using Varied Processing/Fabrication Techniques) Showing the Twin and/or SIM Mechanisms[a]

alloys	processing method	deformation mechanism	$e/\bar{a}$	$\Delta\bar{r} \times 10^{-3}$ nm	refs.
Ti−6Cr−4Mo−2Al−2Sn−1Zr (wt %)	ST	twin and SIM	4.12	−1.2575	60
Ti−8.5Cr−1.5Sn (wt %)	HR	twin and SIM	4.16	−1.4663	61
Ti−7.5Mo (wt %)	HR and ST	twin and SIM	4.08	−0.3110	62
Ti−2Al−9.2Mo−2Fe (wt %)	ST	twin and SIM	4.13	−0.8992	63
Ti−5.3Mo−6.5Sn−10.2Nb−10Zr (wt %)	cast	twin and SIM	4.13	0.7244	64
Ti−25Nb−10Ta−5Zr (wt %)	ST	twin and SIM	4.20	0.2378	65
Ti−29Nb−13Ta−4.6Zr (wt %)	ST	twin and SIM	4.25	0.1752	65
Ti−35Nb−10Ta−5Zr (wt %)	ST	twin and SIM	4.28	0.1832	65
Ti−26Nb (atom %)	ST	twin and SIM	4.26	−0.2596	66
Ti−18Nb−8Zr (atom %)	ST	twin and SIM	4.18	0.8622	66
Ti−16Nb−10Zr (atom %)	ST	twin and SIM	4.16	1.1442	66
Ti−12Mo (wt %)	ST and CR	twin and SIM	4.13	−0.5096	67
Ti−25Ta−25Nb (wt %)	CT and ST	twin and SIM	4.28	−0.2805	68
Ti−35Nb−2Ta−3Zr (wt %)	SLS	twin and SIM	4.23	0.0238	69
Ti−4Mo (wt %)	HR and ST	twin and SIM	4.04	−0.1629	70
Ti−3Al−8Mo−7V−3Cr (wt %)	HR and ST	twin and SIM	4.15	−1.9580	41
Ti−10V−4Cr−1Al (wt %)	CR and ST	twin and SIM	4.32	−2.4176	71
Ti−36Nb−2Ta−3Zr (wt %)	annealed	twin and SIM	4.24	0.0174	13
Ti−10V−3Fe−3Al (wt %)	HR and ST	twin and SIM	4.14	−1.9493	72
Ti−27.96Nb−11.97Ta−5.02Zr (wt %)	CR and ST	twin and SIM	4.23	0.2216	73
Ti−34Nb (atom %)	HR and ST	twin and SIM	4.34	−0.3400	74
Ti−25Nb−0.7Ta−2Zr (atom %)	CR	twin and SIM	4.26	0.0039	75
Ti−25Nb−10Ta−5Zr (wt %)	powder metallurgy and HT	twin or SIM	4.20	0.2378	52

[a]Note that hot-rolling, cold-rolling, solution treating, selective laser sintering, heat treatment, and stress-induced martensite are abbreviated as HR, CR, ST, SLS, HT, and SIM, respectively.

twinning is possible in these alloys. This phenomenon can be seen in many titanium alloys demonstrating the twin mechanism despite comprising $e/\bar{a}$ values greater than 4.20 (Figure 3).

Figure 3 shows that although titanium alloys, i.e., Ti−10V−4Cr−1Al (wt %)[71] and Ti−34Nb (atom %),[74] lie in the twin region, these alloys possess $e/\bar{a}$ values greater than 4.30. This suggests that despite comprising $e/\bar{a}$ values greater than 4.30, these alloys still possess low stacking fault energy to trigger the formation of twin boundaries. It is also worth noting that Ti−10V−4Cr−1Al (wt %) shows twinning at the $e/\bar{a}$and $\Delta\bar{r}$ values of 4.32 and -2.4×10^{-3} nm, respectively, whereas Ti−5Al−5Mo−5V−3Cr−0.5Fe (wt %),[36] Ti−5Al−5Mo−5V−3Cr (wt %),[41] and Ti−4Al−7Mo−3V−3Cr (wt %)[41] show the slip by contrast at the $e/\bar{a}$and $\Delta\bar{r}$ values of 4.08 and -1.8×10^{-3} nm, 4.06 and -1.7×10^{-3} nm, and 4.08 and -1.5×10^{-3} nm. These alloys show contrasting results than the conventional limits of $e/\bar{a}$ and $\Delta\bar{r}$ for twinning in titanium alloys ($e/\bar{a} < 4.20$ and $\Delta\bar{r}$ close to 0 nm) because of using different processing parameters/techniques. In Ti−10V−4Cr−1Al (wt %), the twinning-induced plasticity and transformation-induced plasticity effects have been observed following the martensitic transformation of the orthorhombic α'' phase. Therefore, Ti−10V−4Cr−1Al (wt %) displays exceptional mechanical properties at an $e/\bar{a}$of 4.32 including a yield strength of 420 MPa, an ultimate tensile strength of 1200 MPa, and a uniform elongation of 35%.[71] Similar kinds of results have also been reported in other research.[78]

4. CONCLUSIONS

The revised $e/\bar{a}$ versus $\Delta\bar{r}$ diagram has been proposed to predict the occurrence of twinning in titanium alloys considering the previously reported results of titanium alloys fabricated using various processing methods. The revised $e/\bar{a}$ versus $\Delta\bar{r}$ diagram suggests that the slip is also possible below the $e/\bar{a}$ value of 4.10 and the twin is also possible above the $e/\bar{a}$ value of 4.20. Furthermore, the parameter $\Delta\bar{r}$ is also important in predicting the occurrence of twinning other than $e/\bar{a}$. It has also been observed that the chances of the twin formation in titanium alloys remain high for $e/\bar{a}$ values between 4.10 and 4.30 and $\Delta\bar{r}$ values between -1×10^{-3} and 1×10^{-3} nm. Therefore, the maximum limit for the occurrence of twinning is found to be up to the $e/\bar{a}$ value of 4.30 in this work and should not be up to the $e/\bar{a}$ value of 4.20. The revised $e/\bar{a}$ versus $\Delta\bar{r}$ diagram is helpful to predict the deformation mechanism when designing new titanium alloys for industry applications.

AUTHOR INFORMATION

Corresponding Author

Chirag Dhirajlal Rabadia − *School of Engineering, Edith Cowan University, Perth, Western Australia 6027, Australia; School of Mechanical Engineering, Engineering Institute of Technology, West Perth, Western Australia 6005, Australia;* orcid.org/0000-0002-3490-8493; Phone: +61 415770505; Email: chiragrabadia@gmail.com, chirag.rabadia@eit.edu.au

Authors

Syed Faraz Jawed − *Faculty of Engineering Science Technology & Management, Ziauddin University, Karachi, Sindh 74600, Pakistan*

Jincheng Wang − *School of Engineering, Edith Cowan University, Perth, Western Australia 6027, Australia; School of Engineering, The University of Western Australia, Perth, Western Australia 6009, Australia*

https://doi.org/10.1021/acsomega.1c05474
ACS Omega 2021, 6, 34056−34064

Milind Siddhpura − *School of Mechanical Engineering, Engineering Institute of Technology, West Perth, Western Australia 6005, Australia*
Arti Siddhpura − *School of Mechanical Engineering, Engineering Institute of Technology, West Perth, Western Australia 6005, Australia*

Complete contact information is available at: https://pubs.acs.org/10.1021/acsomega.1c05474

Notes

The authors declare no competing financial interest.

■ ACKNOWLEDGMENTS

The authors would like to acknowledge the financial support provided by the Engineering Institute of Technology, WA, Australia for open access publication.

■ REFERENCES

(1) Zhang, L. C.; Chen, L. Y. A Review on Biomedical Titanium Alloys: Recent Progress and Prospect. *Adv. Eng. Mater.* **2019**, *21*, 1801215.
(2) Carrozza, A.; Aversa, A.; Fino, P.; Lombardi, M. A study on the microstructure and mechanical properties of the Ti-6Al-2Sn-4Zr-6Mo alloy produced via Laser Powder Bed Fusion. *J. Alloys Compd.* **2021**, *870*, 159329.
(3) Wang, J. C.; Liu, Y. J.; Qin, P.; Liang, S. X.; Sercombe, T. B.; Zhang, L. C. Selective laser melting of Ti−35Nb composite from elemental powder mixture: Microstructure, mechanical behavior and corrosion behavior. *Mater. Sci. Eng., A* **2019**, *760*, 214−224.
(4) Rabadia, C. D.; Liu, Y. J.; Zhao, C. H.; Wang, J. C.; Jawed, S. F.; Wang, L. Q.; Chen, L. Y.; Sun, H.; Zhang, L. C. Improved trade-off between strength and plasticity in titanium based metastable beta type Ti-Zr-Fe-Sn alloys. *Mater. Sci. Eng., A* **2019**, *766*, 138340.
(5) Jawed, S. F.; Rabadia, C. D.; Liu, Y. J.; Wang, L. Q.; Li, Y. H.; Zhang, X. H.; Zhang, L. C. Beta-type Ti-Nb-Zr-Cr alloys with large plasticity and significant strain hardening. *Mater. Des.* **2019**, *181*, 108064.
(6) (a) Wang, J.; Liu, Y.; Rabadia, C. D.; Liang, S.-X.; Sercombe, T. B.; Zhang, L.-C. Microstructural homogeneity and mechanical behavior of a selective laser melted Ti-35Nb alloy produced from an elemental powder mixture. *J. Mater. Sci. Technol.* **2021**, *61*, 221−233. (b) Rabadia, C. D.; Liu, Y. J.; Jawed, S. F.; Wang, L. Q.; Sun, H.; Zhang, L. C. Deformation and toughness behavior of β-type titanium alloys comprising C15-type Laves phase. *Mater. Today Sustainability* **2020**, *9*, 100034. (c) Huang, S.; Zhao, Q.; Wu, C.; Lin, C.; Zhao, Y.; Jia, W.; Mao, C. Effects of β-stabilizer elements on microstructure formation and mechanical properties of titanium alloys. *J. Alloys Compd.* **2021**, *876*, 160085. (d) Hong, S. H.; Park, S. W.; Park, C. H.; Yeom, J.-T.; Kim, K. B. Relationship between phase stability and mechanical properties on near/metastable β-type Ti−Cr-(Mn) cast alloys. *J. Alloys Compd.* **2020**, *821*, 153516.
(7) (a) Rabadia, C. D.; Liu, Y. J.; Chen, L. Y.; Jawed, S. F.; Wang, L. Q.; Sun, H.; Zhang, L. C. Deformation and strength characteristics of Laves phases in titanium alloys. *Mater. Des.* **2019**, *179*, 107891. (b) Zhang, L. C.; Liu, Y.; Li, S.; Hao, Y. Additive Manufacturing of Titanium Alloys by Electron Beam Melting: A Review. *Adv. Eng. Mater.* **2018**, *20*, 1700842. (c) Wang, L.; Xie, L.; Lv, Y.; Zhang, L.; Chen, L.; Meng, Q.; Qu, J.; Zhang, D.; Lu, W. Microstructure evolution and superelastic behavior in Ti-35Nb-2Ta-3Zr alloy processed by friction stir processing. *Acta Mater.* **2017**, *131*, 499−510. (d) Hwang, Y. J.; Hong, S. H.; Kim, Y. S.; Park, H. J.; Jeong, Y. B.; Kim, J. T.; Kim, K. B. Influence of silicon content on microstructure and mechanical properties of Ti-Cr-Si alloys. *J. Alloys Compd.* **2018**, *737*, 53−57. (e) Rabadia, C. D.; Liu, Y.; Jawed, S. F.; Wang, L.; Zhang, L. Bulk deformation and toughness behavior of titanium alloys comprising the C15-type Laves and beta phases. International Conference on Materials Science and Engineering-2019, Melbourne.
(8) Bahl, S.; Meka, S. R. K.; Suwas, S.; Chatterjee, K. Surface Severe Plastic Deformation of an Orthopedic Ti−Nb−Sn Alloy Induces Unusual Precipitate Remodeling and Supports Stem Cell Osteogenesis through Akt Signaling. *ACS Biomater. Sci. Eng.* **2018**, *4*, 3132−3142.
(9) Li, H. Y.; Qiao, J. W.; Wang, Z.; Shi, X. H.; Yang, H. J.; Wu, Y. C. A semi-empirical model for predicting yielding in metallic glass matrix composites. *Scr. Mater.* **2019**, *170*, 71−75.
(10) Zhu, Y. T.; Liao, X. Z.; Wu, X. L. Deformation twinning in nanocrystalline materials. *Prog. Mater. Sci.* **2012**, *57*, 1−62.
(11) Bignon, M.; Bertrand, E.; Rivera-Díaz-del-Castillo, P. E. J.; Tancret, F. Martensite formation in titanium alloys: Crystallographic and compositional effects. *J. Alloys Compd.* **2021**, *872*, 159636.
(12) Christian, J. W.; Mahajan, S. Deformation twinning. *Prog. Mater. Sci.* **1995**, *39*, 1−157.
(13) Lai, M. J.; Tasan, C. C.; Raabe, D. On the mechanism of {332} twinning in metastable β titanium alloys. *Acta Mater.* **2016**, *111*, 173−186.
(14) Tiwary, C. S.; Paliwal, M.; Kashyap, S.; Pandey, P.; Sarkar, S.; Kundu, I.; Bhaskar, S.; Jung, I.-H.; Chattopadhyay, K.; Banerjee, D. Microstructures and mechanical properties of ternary Ti−Si−Sn alloys. *Mater. Sci. Eng., A* **2020**, *770*, 138472.
(15) Tiwary, C. S.; Pandey, P.; Sarkar, S.; Das, R.; Samal, S.; Biswas, K.; Chattopadhyay, K. Five decades of research on the development of eutectic as engineering materials. *Prog. Mater. Sci.* **2022**, *123*, 100793.
(16) Rabadia, C. D. Microstructure and mechanical behavior of metastable beta type titanium alloys, 2020. https://ro.ecu.edu.au/theses/2278/.
(17) Katiyar, N. K.; Biswas, K.; Tiwary, C. S. Cryomilling as environmentally friendly synthesis route to prepare nanomaterials. *Int. Mater. Rev.* **2021**, *66*, 493−532.
(18) Bahrami, A.; Ying, P.; Wolff, U.; Rodríguez, N. P.; Schierning, G.; Nielsch, K.; He, R. Reduced Lattice Thermal Conductivity for Half-Heusler ZrNiSn through Cryogenic Mechanical Alloying. *ACS Appl. Mater. Interfaces* **2021**, *13*, 38561−38568.
(19) Wang, C. H.; Russell, A. M.; Cao, G. H. A semi-empirical approach to the prediction of deformation behaviors of β-Ti alloys. *Scr. Mater.* **2019**, *158*, 62−65.
(20) Abdel-Hady, M.; Hinoshita, K.; Morinaga, M. General approach to phase stability and elastic properties of β-type Ti-alloys using electronic parameters. *Scr. Mater.* **2006**, *55*, 477−480.
(21) Morinaga, M.; Kato, M.; Kamimura, T.; Fukumoto, M.; Harada, I.; Kubo, K. Theoretical Design of Beta-Type Titanium-Alloys. In *Titanium 92: Science and Technology*; Froes, F., Caplan, I., Eds.; Minerals, Metals & Materials Soc: Warrendale, PA: San Diego, CA, 1993; Vol. *1*−*3*; pp 217−224.
(22) Jawed, S. F.; Liu, Y. J.; Wang, J. C.; Rabadia, C. D.; Wang, L. Q.; Li, Y. H.; Zhang, X. H.; Zhang, L. C. Tailoring deformation and superelastic behaviors of beta-type Ti-Nb-Mn-Sn alloys. *J. Mech. Behav. Biomed. Mater.* **2020**, *110*, 103867.
(23) Ma, X. M.; Sun, W. Characterization of deformation localization in cold-rolled metastable β-Ti−Nb−Ta−Zr alloy. *J. Alloys Compd.* **2011**, *509*, S294−S298.
(24) Rabadia, C. D.; Liu, Y. J.; Jawed, S. F.; Wang, L.; Li, Y. H.; Zhang, X. H.; Sercombe, T. B.; Sun, H.; Zhang, L. C. Improved deformation behavior in Ti-Zr-Fe-Mn alloys comprising the C14 type Laves and β phases. *Mater. Des.* **2018**, *160*, 1059−1070.
(25) Rabadia, C. D.; Liu, Y. J.; Wang, L.; Sun, H.; Zhang, L. C. Laves phase precipitation in Ti-Zr-Fe-Cr alloys with high strength and large plasticity. *Mater. Des.* **2018**, *154*, 228−238.
(26) Sandlöbes, S.; Korte-Kerzel, S.; Raabe, D. On the influence of the heat treatment on microstructure formation and mechanical properties of near-α Ti-Fe alloys. *Mater. Sci. Eng., A* **2019**, *748*, 301−312.
(27) Biesiekierski, A.; Wang, J.; Abdel-Hady Gepreel, M.; Wen, C. A new look at biomedical Ti-based shape memory alloys. *Acta Biomater.* **2012**, *8*, 1661−1669.
(28) Jawed, S. F.; Rabadia, C. D.; Liu, Y. J.; Wang, L. Q.; Qin, P.; Li, Y. H.; Zhang, X. H.; Zhang, L. C. Strengthening mechanism and corrosion resistance of beta-type Ti-Nb-Zr-Mn alloys. *Mater. Sci. Eng., C* **2020**, *110*, 110728.

(29) Ikehata, H.; Nagasako, N.; Furuta, T.; Fukumoto, A.; Miwa, K.; Saito, T. First-principles calculations for development of low elastic modulus Ti alloys. *Phys. Rev. B* **2004**, *70*, 174113.
(30) Ye, Y. F.; Liu, C. T.; Yang, Y. A geometric model for intrinsic residual strain and phase stability in high entropy alloys. *Acta Mater.* **2015**, *94*, 152−161.
(31) Varvenne, C.; Leyson, G. P. M.; Ghazisaeidi, M.; Curtin, W. A.; Huang, Y.; Yang, Y.; Wang, J.; Liu, C. T. Solute strengthening in random alloysAtomic-size effect and solid solubility of multicomponent alloys. *Acta Mater.* **2017**, *124*, 660−683.
(32) Hanada, S.; Izumi, O. Deformation behaviour of retained β phase in β-eutectoid Ti-Cr alloys. *J. Mater. Sci.* **1986**, *21*, 4131−4139 journal article.
(33) Lai, M. J.; Tasan, C. C.; Raabe, D. Deformation mechanism of ω-enriched Ti−Nb-based gum metal: Dislocation channeling and deformation induced $\omega-\beta$ transformation. *Acta Mater.* **2015**, *100*, 290−300.
(34) Gysler, A.; Lütjering, G.; Gerold, V. Deformation behavior of age-hardened Ti-Mo alloys. *Acta Metall.* **1974**, *22*, 901−909.
(35) Min, X. H.; Emura, S.; Sekido, N.; Nishimura, T.; Tsuchiya, K.; Tsuzaki, K. Effects of Fe addition on tensile deformation mode and crevice corrosion resistance in Ti−15Mo alloy. *Mater. Sci. Eng., A* **2010**, *527*, 2693−2701.
(36) Fan, J.; Kou, H.; Zhang, Y.; Germain, L.; Hua, K.; Tang, L.; Esling, C.; Li, J. Formation of slip bands and microstructure evolution of Ti-5Al-5Mo-5V-3Cr-0.5Fe alloy during warm deformation process. *J. Alloys Compd.* **2019**, *770*, 183−193.
(37) Rabadia, C. D.; Liu, Y. J.; Cao, G. H.; Li, Y. H.; Zhang, C. W.; Sercombe, T. B.; Sun, H.; Zhang, L. C. High-strength β stabilized Ti-Nb-Fe-Cr alloys with large plasticity. *Mater. Sci. Eng., A* **2018**, *732*, 368−377.
(38) Fernandes Santos, P.; Niinomi, M.; Liu, H.; Cho, K.; Nakai, M.; Trenggono, A.; Champagne, S.; Hermawan, H.; Narushima, T. Improvement of microstructure, mechanical and corrosion properties of biomedical Ti-Mn alloys by Mo addition. *Mater. Des.* **2016**, *110*, 414−424.
(39) Jawed, S. F.; Rabadia, C. D.; Liu, Y. J.; Wang, L. Q.; Li, Y. H.; Zhang, X. H.; Zhang, L. C. Mechanical characterization and deformation behavior of β-stabilized Ti-Nb-Sn-Cr alloys. *J. Alloys Compd.* **2019**, *792*, 684−693.
(40) Min, X. H.; Emura, S.; Nishimura, T.; Tsuchiya, K.; Tsuzaki, K. Microstructure, tensile deformation mode and crevice corrosion resistance in Ti−10Mo−xFe alloys. *Mater. Sci. Eng., A* **2010**, *527*, 5499−5506.
(41) Sadeghpour, S.; Abbasi, S. M.; Morakabati, M.; Kisko, A.; Karjalainen, L. P.; Porter, D. A. On the compressive deformation behavior of new beta titanium alloys designed by d-electron method. *J. Alloys Compd.* **2018**, *746*, 206−217.
(42) Hanada, S.; Yoshio, T.; Izumi, O. Plastic deformation mode of retained β phase in β-eutectoid Ti-Fe alloys. *J. Mater. Sci.* **1986**, *21*, 866−870 journal article.
(43) Takemoto, Y.; Shimizu, I.; Sakakibara, A.; Hida, M.; Mantani, Y. Tensile behavior and cold workability of Ti-Mo alloys. *Mater. Trans.* **2004**, *45*, 1571−1576.
(44) Yang, R.; Rahman, K. M.; Rakhymberdiyev, A. N.; Dye, D.; Vorontsov, V. A. Mechanical behaviour of Ti-Nb-Hf alloys. *Mater. Sci. Eng., A* **2019**, *740-741*, 398−409.
(45) Min, X.; Chen, X.; Emura, S.; Tsuchiya, K. Mechanism of twinning-induced plasticity in β-type Ti−15Mo alloy. *Scr. Mater.* **2013**, *69*, 393−396.
(46) Ozan, S.; Li, Y.; Lin, J.; Zhang, Y.; Jiang, H.; Wen, C. Microstructural evolution and its influence on the mechanical properties of a thermomechanically processed β Ti−32Zr−30Nb alloy. *Mater. Sci. Eng., A* **2018**, *719*, 112−123.
(47) Zhan, H.; Zeng, W.; Wang, G.; Kent, D.; Dargusch, M. On the deformation mechanisms and strain rate sensitivity of a metastable β Ti−Nb alloy. *Scr. Mater.* **2015**, *107*, 34−37.
(48) Wang, X. L.; Li, L.; Xing, H.; Ou, P.; Sun, J. Role of oxygen in stress-induced ω phase transformation and $\{332\}\langle 113\rangle$ mechanical twinning in βTi−20V alloy. *Scr. Mater.* **2015**, *96*, 37−40.
(49) Ji, X.; Emura, S.; Min, X.; Tsuchiya, K. Strain-rate effect on work-hardening behavior in β-type Ti-10Mo-1Fe alloy with TWIP effect. *Mater. Sci. Eng., A* **2017**, *707*, 701−707.
(50) Sun, B.; Meng, X. L.; Gao, Z. Y.; Cai, W. Study on the deformation mechanism of the martensitic Ti−16Nb high temperature shape memory alloy. *Mater. Sci. Eng., A* **2019**, *742*, 590−596.
(51) Fitzner, A.; Prakash, D. G. L.; da Fonseca, J. Q.; Thomas, M.; Zhang, S.-Y.; Kelleher, J.; Manuel, P.; Preuss, M. The effect of aluminium on twinning in binary alpha-titanium. *Acta Mater.* **2016**, *103*, 341−351.
(52) Sakaguchi, N.; Niinomi, M.; Akahori, T.; Takeda, J.; Toda, H. Relationships between tensile deformation behavior and microstructure in Ti−Nb−Ta−Zr system alloys. *Mater. Sci. Eng., C* **2005**, *25*, 363−369.
(53) Mantri, S. A.; Choudhuri, D.; Alam, T.; Ageh, V.; Sun, F.; Prima, F.; Banerjee, R. Change in the deformation mode resulting from beta-omega compositional partitioning in a TiMo alloy: Room versus elevated temperature. *Scr. Mater.* **2017**, *130*, 69−73.
(54) Reck, A.; Pilz, S.; Kuczyk, M.; Gebert, A.; Zimmermann, M. Cyclic deformation characteristics of the metastable β-type Ti−40Nb alloy. *Mater. Sci. Eng., A* **2019**, *761*, 137966.
(55) Min, X. H.; Tsuzaki, K.; Emura, S.; Tsuchiya, K. Heterogeneous twin formation and its effect on tensile properties in Ti−Mo based β titanium alloys. *Mater. Sci. Eng., A* **2012**, *554*, 53−60.
(56) Min, X.; Emura, S.; Meng, F.; Mi, G.; Tsuchiya, K. Mechanical twinning and dislocation slip multilayered deformation microstructures in β-type Ti−Mo base alloy. *Scr. Mater.* **2015**, *102*, 79−82.
(57) Chen, W.; Cao, S.; Kou, W.; Zhang, J.; Wang, Y.; Zha, Y.; Pan, Y.; Hu, Q.; Sun, Q.; Sun, J. Origin of the ductile-to-brittle transition of metastable β-titanium alloys: Self-hardening of ω-precipitates. *Acta Mater.* **2019**, *170*, 187−204.
(58) Mythili, R.; Saroja, S.; Vijayalakshmi, M. Study of mechanical behavior and deformation mechanism in an $\alpha-\beta$ Ti−4.4Ta−1.9Nb alloy. *Mater. Sci. Eng., A* **2007**, *454-455*, 43−51.
(59) Zhu, Y.; Wang, L.; Wang, M.; Liu, Z.; Qin, J.; Zhang, D.; Lu, W. Superelastic and shape memory properties of Ti x Nb3Zr2Ta alloys. *J. Mech. Behav. Biomed.* **2012**, *12*, 151−159.
(60) Ren, L.; Xiao, W.; Ma, C.; Zheng, R.; Zhou, L. Development of a high strength and high ductility near β-Ti alloy with twinning induced plasticity effect. *Scr. Mater.* **2018**, *156*, 47−50.
(61) Yang, H.; Wang, D.; Zhu, X.; Fan, Q. Dynamic compression-induced twins and martensite and their combined effects on the adiabatic shear behavior in a Ti-8.5Cr-1.5Sn alloy. *Mater. Sci. Eng., A* **2019**, *759*, 203−209.
(62) Ji, X.; Emura, S.; Liu, T.; Suzuta, K.; Min, X.; Tsuchiya, K. Effect of oxygen addition on microstructures and mechanical properties of Ti-7.5Mo alloy. *J. Alloys Compd.* **2018**, *737*, 221−229.
(63) Xiao, J. F.; Nie, Z. H.; Tan, C. W.; Zhou, G.; Chen, R.; Li, M. R.; Yu, X. D.; Zhao, X. C.; Hui, S. X.; Ye, W. J.; et al. Effect of reverse β-to-ω transformation on twinning and martensitic transformation in a metastable β titanium alloy. *Mater. Sci. Eng., A* **2019**, *759*, 680−687.
(64) Jiang, B.; Wang, Q.; Wen, D.; Xu, F.; Chen, G.; Dong, C.; Sun, L.; Liaw, P. K. Effects of Nb and Zr on structural stabilities of Ti-Mo-Sn-based alloys with low modulus. *Mater. Sci. Eng., A* **2017**, *687*, 1−7.
(65) Hagihara, K.; Nakano, T. Experimental clarification of the cyclic deformation mechanisms of β-type Ti−Nb−Ta−Zr-alloy single crystals developed for the single-crystalline implant. *Int. J. Plast.* **2017**, *98*, 27−44.
(66) Zhang, J.; Sun, F.; Hao, Y.; Gozdecki, N.; Lebrun, E.; Vermaut, P.; Portier, R.; Gloriant, T.; Laheurte, P.; Prima, F. Influence of equiatomic Zr/Nb substitution on superelastic behavior of Ti−Nb−Zr alloy. *Mater. Sci. Eng., A* **2013**, *563*, 78−85.
(67) Sun, F.; Zhang, J. Y.; Marteleur, M.; Gloriant, T.; Vermaut, P.; Laillé, D.; Castany, P.; Curfs, C.; Jacques, P. J.; Prima, F. Investigation of early stage deformation mechanisms in a metastable β titanium alloy

https://doi.org/10.1021/acsomega.1c05474
ACS Omega 2021, 6, 34056−34064

showing combined twinning-induced plasticity and transformation-induced plasticity effects. *Acta Mater.* **2013**, *61*, 6406−6417.
(68) Bertrand, E.; Castany, P.; Gloriant, T. Investigation of the martensitic transformation and the damping behavior of a superelastic Ti−Ta−Nb alloy. *Acta Mater.* **2013**, *61*, 511−518.
(69) Hafeez, N.; Liu, S.; Lu, E.; Wang, L.; Liu, R.; lu, W.; Zhang, L.-C. Mechanical behavior and phase transformation of β-type Ti-35Nb-2Ta-3Zr alloy fabricated by 3D-Printing. *J. Alloys Compd.* **2019**, *790*, 117−126.
(70) Tarzimoghadam, Z.; Sandlöbes, S.; Pradeep, K. G.; Raabe, D. Microstructure design and mechanical properties in a near-α Ti−4Mo alloy. *Acta Mater.* **2015**, *97*, 291−304.
(71) Lilensten, L.; Danard, Y.; Brozek, C.; Mantri, S.; Castany, P.; Gloriant, T.; Vermaut, P.; Sun, F.; Banerjee, R.; Prima, F. On the heterogeneous nature of deformation in a strain-transformable beta metastable Ti-V-Cr-Al alloy. *Acta Mater.* **2019**, *162*, 268−276.
(72) Ahmed, M.; Wexler, D.; Casillas, G.; Ivasishin, O. M.; Pereloma, E. V. The influence of β phase stability on deformation mode and compressive mechanical properties of Ti−10V−3Fe−3Al alloy. *Acta Mater.* **2015**, *84*, 124−135.
(73) Maghsoudlou, A.; Zarei-Hanzaki, A.; Abedi, H. R.; Barabi, A.; Pilehva, F.; Dietrich, D.; Lampke, T. The room temperature tensile deformation behavior of thermomechanically processed β-metastable Ti-Nb-Ta-Zr bio-alloy: the role of deformation-induced martensite. *Mater. Sci. Eng., A* **2018**, *738*, 15−23.
(74) Li, L.; Mei, W.; Xing, H.; Wang, X. L.; Sun, J. Zigzag configuration of mechanical twin and stress-induced omega phase in metastable β Ti−34Nb (at.%) alloy. *J. Alloys Compd.* **2015**, *625*, 188−192.
(75) Lai, M. J.; Li, T.; Raabe, D. ω phase acts as a switch between dislocation channeling and joint twinning- and transformation-induced plasticity in a metastable β titanium alloy. *Acta Mater.* **2018**, *151*, 67−77.
(76) Yao, T.; Du, K.; Wang, H.; Huang, Z.; Li, C.; Li, L.; Hao, Y.; Yang, R.; Ye, H. In situ scanning and transmission electron microscopy investigation on plastic deformation in a metastable β titanium alloy. *Acta Mater.* **2017**, *133*, 21−29.
(77) Gao, J.; Knowles, A. J.; Guan, D.; Rainforth, W. M. ω phase strengthened 1.2GPa metastable β titanium alloy with high ductility. *Scr. Mater.* **2019**, *162*, 77−81.
(78) Liu, Y. J.; Zhang, Y. S.; Zhang, L. C. Transformation-induced plasticity and high strength in beta titanium alloy manufactured by selective laser melting. *Materialia* **2019**, *6*, 100299.

https://doi.org/10.1021/acsomega.1c05474
ACS Omega 2021, 6, 34056−34064